Available online at www.sciencedirect.com
ScienceDirect
Journal of Nuclear Materials 374 (2008) 211–219
journal of nuclear materials
www.elsevier.com/locate/jnucmat

Modeling of oxidation of structural materials in LBE systems

H. Steiner, C. Schroer, Z. Voß, O. Wedemeyer, J. Konys *

Forschungszentrum Karlsruhe, Institut für Materialforschung III, P.O. Box 3640, 76021 Karlsruhe, Germany

Received 9 March 2007; accepted 9 July 2007

Abstract

In recent years, liquid metal alloys have been examined in the light of various applications in technical systems the most famous example is the sodium cooled Fast Breeder Reactor. One major problem in non-isothermal heavy liquid metal systems lies in the corrosion of their structural components. The formation of oxide scales on the structural components is considered as a viable measure in limiting the dissolution rates in the hot parts in lead and lead–bismuth loops. Models for oxide scale growth under the action of flowing liquid metals have been implemented in the newly developed code MATLIM, which allow calculating the evolution of the oxide scales on structural materials in multi-modular loops. There are thermo-hydraulic limitations on oxygen supply from the liquid metal to the structural materials, the oxygen mass transfer coefficient in the liquid metal, which depends on the flow conditions, being rate-determining. This seems to explain, for example, why in the first stage of oxidation of stainless steels slowly growing, dense single layer Fe/Cr spinel scales are formed.

1. Introduction

Liquid metal alloys have various applications in technical systems the most famous example being the sodium cooled Fast Breeder Reactor. Recently, Lead–Bismuth Eutectic (LBE) is foreseen as coolant and target for neutron generation in accelerator driven nuclear systems (ADS) [1,2]. Also, Pb–17Li alloy is considered as a coolant and breeding medium in future fusion reactors [3,4]. The advantage of these liquid metal alloys lies in their high thermal conductivity and their relative safety in case of an accident. But a major problem in non-isothermal liquid metal systems lies in the corrosion of their structural components, consisting mainly of ferritic/martensitic and austenitic stainless steels, as the solubility of structural components in the liquid metal depends in general on the temperature.

The formation of oxide scales on the structural components is considered as a viable means in limiting the dissolution rates in the hot parts of the system, as the solubility of the oxides is in general much smaller than that of the metal alloys [5,6]. Oxide scales might not be stable as for example in Pb–17Li alloy, but there may also be a problem in LBE loops at low oxygen concentrations. Hence, the prediction of the oxide scale evolution is of great importance. Also precipitation of oxides at cooler parts of the system can have consequences as there may be clogging and plugging of components having small cross sections. This may also affect the maintenance and repair of the system as in an accelerator driven nuclear system and in a fusion reactor there will be activation of steel components and there will be transport and deposition of activated material.

Concepts of oxygen control in Pb and Pb–Bi loops had already been developed in Russia some years ago [7,8]. Oxygen control in the loop can only be of practical use if the oxygen activity in the liquid metal is high enough for oxide scale formation on structural components as is the case for Pb and Pb–Bi alloys [9]. From Pb loops it is also known that there is a critical oxygen level below which no oxide scale is formed and dissolution attack of the metal alloy occurs [8]. In this paper we are mainly dealing with oxygen control in an eutectic lead–bismuth system (LBE) like the CORRIDA loop of KALLA lab at Forschungszentrum Karlsruhe (FZK). An oxygen control system requires

* Corresponding author.
E-mail address: juergen.konys@imf.fzk.de (J. Konys).

0022-3115/$ - see front matter © 2007 Elsevier B.V. All rights reserved.
doi:10.1016/j.jnucmat.2007.07.022

Nomenclature

T	temperature
t	time
x	axial position
c	concentration
p	pressure
v, u	velocity
D	diffusivity
$\hat{K}$	mass transfer coefficient
K, k	oxidation rate constants
d	diameter
A	area
U	circumference
R	gas constant
M	atomic weight
P	porosity
L	length
ΔG	free energy of formation
p	pressure
a	activity
ν	kinematic viscosity
ρ	density
δ	layer thickness
σ	surface tension
j	mass flux
b	dissolution/precipitation rate
y	mol fraction

Superscripts and subscripts

w	wall
b	bulk
p	particle
hyd	hydraulic
fl	fluid or flow
ch	channel
O	oxygen
Fe	iron
Cr	chromium
Pb	lead
ox	oxide
ox.m.	oxide scale mass
me	metal
s.l.	surface layer
s	saturation or surface
la	laminar
turb	turbulent
ma	magnetite
sp	spinel
o.c.s.	oxygen control system
reac.	reaction
crit	critical

the continuous measurement of the oxygen activity in the liquid metal [10,11]. It must be assured that no oxides of the liquid metal itself are formed; otherwise the loop can be clogged.

The locations of dissolution and precipitation are mainly determined by the temperature dependence of the solubility of the oxides or of the metal alloys if no oxide scale is present. This means that we have dissolution in the hot parts of the system and precipitation in the cold parts, irrespective of the nature of the dissolution process, whether it is exothermic or endothermic. Depending on the local oxygen concentration at the surface of the structural component there can be duplex scale formation or formation of a single layer Fe/Cr spinel scale with the iron solubility depending on the nature of the oxide scale. Thus, it is indispensable to calculate the axial profiles of oxygen concentration in the bulk of the fluid and at the surface of the structural components. It is in general not sufficient to use only the value of oxygen activity level given by the oxygen control system. Besides dissolution/precipitation processes there may also be diffusion of metallic components through the oxide scale from the steel towards the liquid metal but liquid metal components can also be transported into the oxide scale eventually providing fast diffusion paths for the steel components.

In two previous papers [12,13] information on a recently developed computer code (MATLIM) for the calculation of iron mass transfer in a liquid metal loop was given. The code is meant to deal with multi-modular liquid metal systems, e.g. the two HLM loops operated at FZK, namely PICOLO and CORRIDA (see Ref. [14]). In this report focus is laid on the modeling aspects of oxygen behavior and oxide scale formation and growth. We are going to discuss the implementation of the respective models in the recently developed computer code MATLIM in more detail.

2. Oxygen mass balance

We are not going to derive (exact) solutions for the oxygen concentration in the loop as has for example been tried in Ref. [15], but we will describe oxygen behavior with the help of two characteristic values, namely c_O^b and c_O^w. The parameter c_O^b represents the mean value of the oxygen concentration over the cross section of the coolant channel at an axial position x and the parameter c_O^w the oxygen concentration at the channel walls. Under turbulent flow conditions the oxygen distribution in the coolant channel is rather flat except in a very thin boundary layer of a few microns as the Schmidt-number is in the order of 10^3. In this case the mean oxygen concentration is very near to

the oxygen concentration in the bulk of the fluid. The two characteristic values of oxygen concentration in the liquid metal are linked by the oxygen mass transfer coefficient. This parameter can be calculated with the help of empirical correlations depending on the oxygen diffusion coefficient and thermo-hydraulic parameters (see also Ref. [16]). In this way we have a sound experimental basis for our model.

Approximating the velocity profile in the cross section of the coolant channel by the mean velocity of the fluid u_{fl} (the so-called flow velocity) one can derive simple differential equations for the mean values of the solute concentrations (see Refs. [12–14]). In the meantime we have also included in these differential equations the effect of (oxide) particles in the liquid metal. Thus, the mass balance for the oxygen in the bulk of the fluid $c_{\mathrm{O}}^{\mathrm{b}}$ reads as follows:

$$\frac{\partial c_{\mathrm{O}}^{\mathrm{b}}(t,x)}{\partial t} + u_{\mathrm{fl}} \cdot \frac{\partial c_{\mathrm{O}}^{\mathrm{b}}(t,x)}{\partial x} = \frac{U_{\mathrm{ch}}}{A_{\mathrm{ch}}} \cdot j_{\mathrm{O}}^{\mathrm{w}}(t,x) + n_{\mathrm{p}} \cdot A_{\mathrm{p}} \cdot j_{\mathrm{O}}^{\mathrm{p}} \tag{1}$$

n_{p} is the particle density and A_{p} is the particle surface area.

Except for a relatively short period after the start of the operation of the loop and except for special circumstances like a very fast change of the oxygen activity given by the oxygen control system, the partial time derivative of $c_{\mathrm{O}}^{\mathrm{b}}$ can be neglected. In the following we will apply Eq. (1) only for quasi-stationary conditions. That means under conditions slowly varying with time.

According to the Gibbs–Thompson equation, the solubility of a solute i depends on the curvature of the surface. For a spherical particle we have:

$$c_i^{\mathrm{s,p}} = c_i^{\mathrm{s}} \cdot \exp(2 \cdot \sigma_{\mathrm{p}} \cdot M_{\mathrm{p}}/(r_{\mathrm{p}} \cdot \rho_{\mathrm{p}} \cdot R \cdot T) \tag{2}$$

r_{p} is the particle radius and M_{p} is the atomic weight of the particle mass, T is the temperature, R is the general gas constant (8.317 J/K/mol), σ_{p} is the surface tension of the particle and ρ_{p} = mass density of the particle.

Particles in an oversaturated solution can only grow in a stable way by atomic or molecular deposition if the particle radius is above a certain critical limit. Particles below the critical radius are dissolved even in an oversaturated solution. But such particles could, of course, grow by coagulation.

We get for the critical radius of spherical particles the following equation:

$$r_{\mathrm{p}}^{\mathrm{crit}} = \frac{2 \cdot \sigma_{\mathrm{p}} \cdot M_{\mathrm{p}}}{R \cdot T \cdot \rho_{\mathrm{p}} \cdot \ln(c_{\mathrm{Fe}}^{\mathrm{b}}/c_{\mathrm{Fe}}^{\mathrm{s}})} \tag{3}$$

We have not included in Eq. (1) a term for the time variation of the particle density n_{p} as we are for the time being not in a position to describe the relevant processes like spalling of oxide scales, coagulation and trapping of particles, etc. in a quantitative way. Thus, the iron mass equivalent contained in particles, their shape (spherical or cylindrical) and the particle radius must be specified by the user of the code.

The oxygen mass flux to the channel walls $j_{\mathrm{O}}^{\mathrm{w}}$ and to the particles in the fluid $j_{\mathrm{O}}^{\mathrm{p}}$ is linked to the respective iron mass flux in the following way:

$$j_{\mathrm{O}}^{\mathrm{w}} = f_{\mathrm{O}}^{\mathrm{Fe}} \cdot j_{\mathrm{Fe}}^{\mathrm{w}} + f_{\mathrm{ox}}^{\mathrm{me}} j_{\mathrm{ox}} \tag{4}$$

$$j_{\mathrm{O}}^{\mathrm{p}} = f_{\mathrm{O}}^{\mathrm{Fe}} \cdot j_{\mathrm{Fe}}^{\mathrm{p}} \tag{5}$$

In case of duplex scale formation with a magnetite outer subscale and an inner Fe/Cr spinel subscale with the composition $\mathrm{Fe}_{\alpha}\mathrm{Cr}_{\beta}\mathrm{O}_4$ we have the following relations:

$$f_{\mathrm{O}}^{\mathrm{Fe}} = \frac{4 \cdot M_{\mathrm{O}}}{3 \cdot M_{\mathrm{Fe}}} \tag{6}$$

$$f_{\mathrm{ox}}^{\mathrm{me}} = \frac{1}{2} \cdot \left(\frac{4 \cdot M_{\mathrm{O}}}{4 \cdot M_0 + \alpha \cdot M_{\mathrm{Fe}} + \beta \cdot M_{\mathrm{Cr}}} + \frac{4 \cdot M_{\mathrm{O}}}{4 \cdot M_{\mathrm{O}} + 3 \cdot M_{\mathrm{Fe}}} \right) \tag{7}$$

We have also assumed that the channel walls are oxidized. Therefore the mass flux due to oxidation itself j_{ox} appears in Eq. (4). If the growth of the oxide scale is diffusion controlled the oxygen mass flux is inversely proportional to the actual oxide scale thickness:

$$j_{\mathrm{ox}}(t) = \frac{k_{\mathrm{ox.m.}}(T, c_{\mathrm{O}})}{\delta_{\mathrm{ox}}(t)} \tag{8}$$

$k_{\mathrm{ox.m.}}(T, c_{\mathrm{O}})$ is the mass related oxidation rate constant.

As a first approximation we used the oxidation rate constant $k_{\mathrm{ox.m.}}(T, c_{\mathrm{O}})$ data obtained from tests done under gas atmosphere, as the diffusion in the oxide scale should only depend on the conditions in the scale and not on the environment.

The rate of oxygen supplied by the oxygen control system is given as (in wppm/s):

$$\dot{m}_{\mathrm{O}}^{\mathrm{o.c.s.}} = (c_{\mathrm{O}}^{\mathrm{out}} - c_{\mathrm{O}}^{\mathrm{in}}) \cdot u_{\mathrm{fl}}^{\mathrm{o.c.s.}} \cdot A^{\mathrm{o.c.s.}} \tag{9}$$

$A^{\mathrm{o.c.s}}$ is the cross section of the flow channel within the oxygen control system.

Besides dissolution and precipitation of iron oxides like magnetite and Fe/Cr spinel there may also be transport of alloying elements through the oxide scale. Thus, besides Fe and Cr a lot of other metallic elements may be dissolved in the liquid metal. We think that the iron mass flux is the dominating contribution and that with the present model the real situation can be approximated.

3. Oxygen content at the surface of structures

Knowing the oxygen content in the bulk of the fluid $c_{\mathrm{O}}^{\mathrm{b}}$, the oxygen content at the channel wall $c_{\mathrm{O}}^{\mathrm{w}}$ can be calculated with the help of the following equation:

$$j_{\mathrm{O}}^{\mathrm{w}} = \overset{\succ}{K}_{\mathrm{O}} \cdot (c_{\mathrm{O}}^{\mathrm{w}} - c_{\mathrm{O}}^{\mathrm{b}}) \tag{10}$$

The mass transfer coefficient $\overset{\succ}{K}_{\mathrm{O}}$ for oxygen can be calculated in the same way as that for iron (see Refs. [13,16]), we have only to replace the iron diffusion coefficient in LBE by the respective diffusion coefficient for oxygen. For this we have taken the correlation for the oxygen diffusion coefficient in LBE given in Ref. [17]:

$$D_{\mathrm{O}}^{\mathrm{LBE}}(T) = 10^{-0.813-3612./T} \text{ in } \mathrm{cm}^2/\mathrm{s} \tag{11}$$

4. Evolution of oxide scale thickness

The change of the oxide scale thickness in a time increment Δt is given by:

$$\Delta\delta_{ox}(t) = \left(\frac{K(T,c_O)}{2\cdot\delta_{ox}(t)} + b(x)\right)\cdot\Delta t \tag{12}$$

b is the dissolution/precipitation rate of the oxide in cm/s.

$$K(T,c_O) = \frac{2\cdot k_{ox.m.}(T,c_O)}{\rho_{ox}} \tag{13}$$

The parameter b describes the effect of the liquid metal on the oxide scale. In a non-isothermal loop there are axial regions with dissolution of scales (b is negative) and other areas with precipitation (b is positive).

A similar equation has been used by Tedmon [18] to describe high temperature formation of Cr_2O_3 with scale removal due to volatilization. The consequences of scale removal effects on the kinetics of oxidation have also been investigated in Ref. [19]. It was shown that an asymptotic oxide scale thickness will be reached.

We prefer to use an incremental formulation of Tedmon's equation. In this way we can also cope with spalling effects.

5. Solubility product over oxide scales

For the calculation of magnetite dissolution we use the solubility product for iron and oxygen given in Refs. [15,20]:

$$c_{Fe}\cdot c_O^{4/3} = a_{Pb}^{4/3}\cdot 10^{11.35-12844/T} \tag{14}$$

In order to establish the solubility product of a Fe/Cr spinel of the composition $Fe_\alpha Cr_\beta O_4$ we take profit of the work of Li [20]. Thus, the following reaction is to be considered:

$$\frac{1}{4}[y\cdot Fe_3O_4 + (1-y)FeCr_2O_4] + Pb = \left[\frac{1-y}{4}+\frac{3\cdot y}{4}\right]Fe + \frac{1-y}{2}Cr + PbO \tag{15}$$

with:

$$\beta = 2\cdot(1-y) \quad \text{and} \quad \alpha = 2y+1 \tag{16}$$

For this reaction we have to consider the following expression for the free enthalpy:

$$\Delta G_{reac.} = \Delta G_{PbO} - \frac{1}{4}\Delta G_{sp} \tag{17}$$

Considering the Fe/Cr spinel phase as an ideal mixture of Fe_3O_4 and Cr_2FeO_4 with y being the mol fraction of Fe_3O_4:

$$y\cdot Fe_3O_4 + (1-y)\cdot Cr_2FeO_4 \tag{18}$$

the free enthalpy of formation of the Fe/Cr spinel can be calculated as follows:

$$\Delta G_{sp}(T) = y\cdot\Delta G_{Fe_3O_4} + (1-y)\cdot\Delta G_{Cr_2FeO_4} + \Delta G_m \tag{19}$$

with the mixing enthalpy given as:

$$\Delta G_m = R\cdot T\cdot(y\cdot\ln(y) + (1-y)\cdot\ln(1-y)) \tag{20}$$

For the data given in Ref. [21] we obtain for $\alpha = 2.3$ the following expression:

$$\frac{\Delta G_{sp}}{2\cdot R\cdot T} = -\frac{73930.}{T} + 18.94 \tag{21}$$

Applying the mass action law, we obtain:

$$\exp\left(-\frac{\Delta G_{reac.}}{R\cdot T}\right) = \frac{a_{Fe}^{\frac{1-y}{4}+\frac{3y}{4}}\cdot a_{Cr}^{\frac{1-y}{2}}\cdot a_{PbO}}{a_{Pb}} \tag{22}$$

Using for the activities:

$$a_i = \frac{c_i}{c_{i,s}} \tag{23}$$

we obtain for $\alpha = 2.3$ together with the solubility data for Fe, Cr and O given in Ref. [15]:

$$c_{Fe}^{0.575}\cdot c_{Cr}^{0.175}\cdot c_O = a_{Pb}\cdot 10^{\frac{-10981.7}{T}+8.29} \tag{24}$$

It should be noted that in applying the correlations (14) or (24) we have to insert the local value at axial position x of the oxygen concentration at the surface of structural material $c_O^w(x)$.

6. Oxidation correlations for AISI 316L and T91

In the following we are going to give correlations for the oxidation rate constant for AISI 316L and T91. These correlations were obtained from tests done under gas atmospheres. They depend on the temperature and the oxygen partial pressure. We think that as a first approximation they are in this form in principal also applicable in LBE. With experimental data, which we hope to gain from relevant tests in LBE we can check whether this hypothesis is really correct. From the tests done so far under LBE it is not possible to deduce generally applicable correlations for the oxidation rate constants, as the experimental conditions varied considerably and as it is difficult to quantify the scale removal effect of the liquid metal [14] under the different flow conditions. There are, for example, no systematic studies of the influence of the oxygen concentration in the liquid metal and one should note that magnetite subscales are prone to spalling.

6.1. AISI 316L steel

Saito et al. [22] has determined the oxidation rate of AISI 316L for tests under gas atmosphere with the following dependence on the oxygen partial pressure p_{O_2}:

$$K(T,p_{O_2}) = 4.56\cdot 10^{-3}\cdot p_{O_2}^{0.141}\cdot e^{-13708/T} \tag{25}$$

6.2. T91 steel

From the data given in Ref. [23] we have derived the following oxidation rate constant $K(T,p_{O_2})$ for T91:

$$K(T,p_{O_2}) = 0.848\cdot 10^{-1}\cdot e^{-16352/T}\cdot p_{O_2}^{0.11} \tag{26}$$

p_{O_2} in MPa, T in K and K in cm^2/s.

The correlations for both steels are rather similar in their temperature and oxygen partial pressure dependence.

The oxygen partial pressure in LBE is determined by the oxygen content as follows:

$$p_{O_2}^{LBE}(T, c_O) = 0.596 \cdot \exp(-36790./T) \cdot c_O^2 \quad (27)$$

p_{O_2} in MPa and c_O in wppm.

Using this relation we can express the oxide rate constant as a function of temperature and oxygen concentration in the liquid metal.

7. Consequences of thermo-hydraulic limitations on the oxygen supply to structural materials

The oxygen needed for the growth of the oxide scale is supplied by the liquid metal. The main parameter for this is the oxygen mass transfer coefficient. This mass transfer coefficient is determined by the thermo-hydraulic conditions in the loop. Besides, there may be contributions to the oxygen flux coming from dissolution or precipitation of oxide. For dissolution of oxides, oxygen is released into the bulk of the LBE, whereas for precipitation of oxides, oxygen is consumed. Thus, the balance equation for oxygen mass flux needed for oxide scale growth is as follows:

$$\overset{\succ}{K}_O \cdot (c_O^b - c_O^w) + j_O^{diss/precip} = j_{ox} \cdot f_{ox}^{me} \quad (28)$$

$$j_O^{diss} > 0 \quad j_O^{precip} < 0 \quad (29)$$

$j_O^{diss/precip}$ is the oxygen mass flux due to dissolution/precipitation of iron oxides.

Eq. (28) can be considered under two viewpoints: (a) what level of oxygen concentration in the bulk is needed for adjusting a certain value of the oxygen concentration at the surface of the structural materials and (b) whether Eq. (28) has a physical solution at all under the assumed modes of oxidation for a certain value of oxygen concentration in the bulk. One must understand that the oxygen diffusion coefficient in liquid metals is about six orders of magnitude lower than in gas atmospheres. Also, one should note that it is a technical goal to operate LBE loops at rather low levels of oxygen concentrations (0.005–0.01 wppm). This has certain consequences for the formed oxide scales.

The oxygen mass transfer coefficient is especially low under laminar flow conditions and it might be of some interest to compare for this flow regime the situation in a gas atmosphere (steam + oxygen for example) to the situation in a LBE loop like CORRIDA.

We have derived from the work of Fuller et al. [24] the following correlation for the diffusion coefficient of oxygen in steam:

$$D_{H_2O,O_2}(T, p) = 1.251 \cdot 10^{-6} \cdot \frac{T^{1.75}}{p} \quad (30)$$

p is the total gas pressure in MPa and T is the temperature in K.

The oxygen diffusion coefficient in LBE can be calculated with the help of Eq. (11).

Under laminar flow conditions the Sherwood number in a fully circular cross section is 3.66. Neglecting for this case dissolution and precipitation effects we have calculated the oxygen concentration difference in the coolant channel to supply the oxygen mass flux in case of an oxide scale formed on AISI 316L of 1 μm thickness after 1000 h if the oxygen concentration at the surface is at 0.01 wppm. The relevant values are shown in Table 1.

In order to be definite we have used for the calculations the empirical correlation for the oxidation rate constant of AISI 316L given in chapter 6, although it is doubtful, whether it can be applied for such thin oxide scales. Thus, the oxygen concentration difference is much higher in an LBE loop than under gas atmosphere. A value of 0.42 wppm can certainly not be neglected. For turbulent flow and a mass transfer coefficient of 0.0175 cm/s (a value typical for turbulent flow in the test section of CORRIDA) we obtain of course a much lower value for the oxygen difference, namely about 7×10^{-4} wppm.

The oxygen concentration difference depends mainly on the flow regime and on the oxide scale thickness and certainly on the structural features in the oxide scale (density, grain size, etc).

In a situation where precipitation is taking place, the problem with the oxygen difference in the coolant channel would be even more acute, as precipitation consumes oxygen. Thus, except for rather high oxygen activities in LBE, in the low temperature part of the CORRIDA loop only precipitation of oxides on the channel walls and no additional proper oxidation of the structural material is occurring. This conclusion could probably be checked by respective examinations.

In the following we will investigate Eq. (28) under a different aspect, namely we consider turbulent flow in the test section of the CORRIDA loop and ask for the lower boundaries on the oxygen concentration in the bulk of the fluid necessary for duplex scale formation. We neglect dissolution effects, as for the time being we have no experimental values.

The oxygen concentration at the wall cannot fall below the value indicating dissociation of magnetite in case of duplex scale formation:

$$c_O^w \geqslant c_O^{ma} \quad (31)$$

Table 1
Comparison of thermo-physical values relevant for oxidation of AISI 316L after 1000 h in the respective environment

	Gas atmosphere $H_2O + O_2$	LBE
Temperature (K)	823	823
Oxygen diffusion coefficient (cm^2/s)	1.582	6.28×10^{-6}
Oxygen mass transfer coefficient (cm/s)	7.24	2.87×10^{-5}
$c_O^b - c_O^{surf}$ (wppm)	1.6×10^{-6}	0.42

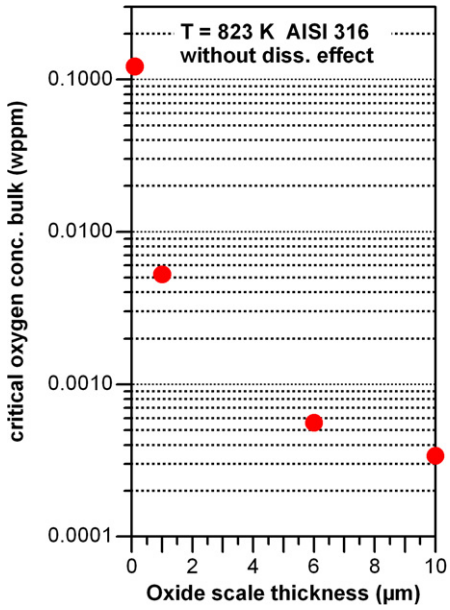

Fig. 1. Critical oxygen concentration in the bulk of the fluid versus oxide scale thickness needed to obtain formation of duplex scales on AISI 316L.

Thus, we have to look for solutions of the following equation:

$$\overset{\succ}{K}_{\mathrm{O}} \cdot (c_{\mathrm{O}}^{\mathrm{b,min}} - c_{\mathrm{O}}^{\mathrm{ma}}) = j_{\mathrm{ox}} \cdot f_{\mathrm{ox}}^{\mathrm{me}} \tag{32}$$

In the test section of the CORRIDA loop we have at 550 °C the following values:

$$\overset{\succ}{K}_{\mathrm{O}} = 0.0175\ \mathrm{cm/s} \quad c_{\mathrm{O}}^{\mathrm{ma}} = 9 \cdot 10^{-5}\ \mathrm{wppm} \tag{33}$$

Eq. (32) has been solved numerically. The values $c_{\mathrm{O}}^{\mathrm{b,min}}$ versus the oxide scale thickness are to be found in Fig. 1.

One can conclude from these results that for an oxygen concentration of 0.005 wppm oxide scale formation cannot start with duplex scale formation. This is impossible due to insufficient oxygen supply. With single layer Fe/Cr spinel formation the oxidation rate constant would be less than one fourth of that for duplex scale formation depending on the structure of the single layer oxide scale. A slowly growing high density scale needs probably a considerably lower oxygen mass flux than a porous oxide scale.

8. Results of calculations with the code MATLIM

The code MATLIM allows a 1-D simulation of multi-modular loops. The relevant differential equations are solved with the help of finite difference techniques by dividing each module into a certain number of axial meshes. In the actual version of the code a mesh length of 1 cm is used allowing integer mesh numbers for all modules of the loop. Specific values for the relevant parameters can be assigned for each axial mesh. Calculations were done for e.g. the CORRIDA loop, which is operated with LBE as a coolant [12–14,25]. The main characteristics of this loop are

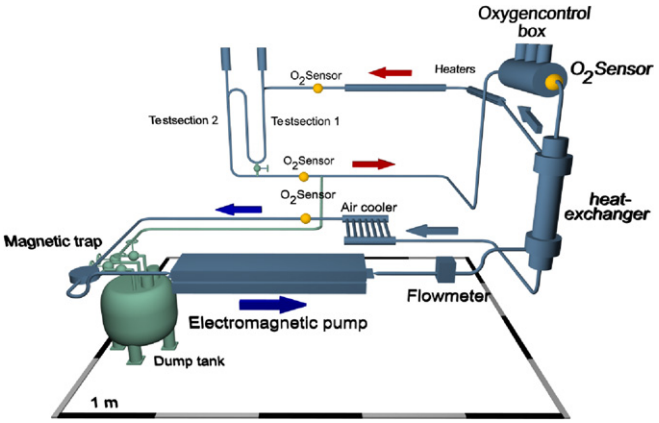

Fig. 2. Schematic view of the CORRIDA loop.

described in Ref. [25]. For the convenience of the reader we have included a schematic representation of the loop (Fig. 2). The loop contains among other modules two test sections and an oxygen control system. The oxygen control system consists of a tank, which is located downstream of the test sections. The liquid metal flows through the tank together with an oxygen-containing gas stream.

There are mainly three different types of physical properties and parameters, which determine material behavior in a liquid metal system. The first group concerns the thermo-hydraulic data of the system like the flow velocity and the hydraulic diameter but also the temperature distribution along the system. The second group concerns material data like viscosity of the liquid metal, diffusivity and solubility of the solutes. The third group encompasses properties of the structural material itself like oxidation rates.

For the calculations we have assumed that the structural material and the specimens in the test sections consist of AISI 316L and we have covered an operation period of 1000 h. For the oxygen concentration supplied by the oxygen control system we have taken three different set values, namely 0.05, 0.01 and 0.005 wppm in order to investigate the response of the loop as simulated by the MATLIM code. For all the calculations we have firstly assumed duplex scale formation on the structural material. Thus, only magnetite will be dissolved and precipitated. The treatment for single oxide layer formation, like it is typical for fast flowing LBE systems, will be part of future investigations.

The single most important thermo-hydraulic parameter is the mass transfer coefficient for the solutes of interest. In our case it is that of oxygen. The mass transfer coefficient depends on the temperature and on hydraulic parameters like the flow velocity and the hydraulic diameter (see also Ref. [16]). Information on this can be found in Figs. 3 and 4. Fig. 3 gives also some evidence about the simulation of the CORRIDA loop features with its different modules within the frame of the MATLIM code. The flow velocity in the test sections is typically 2 m/s.

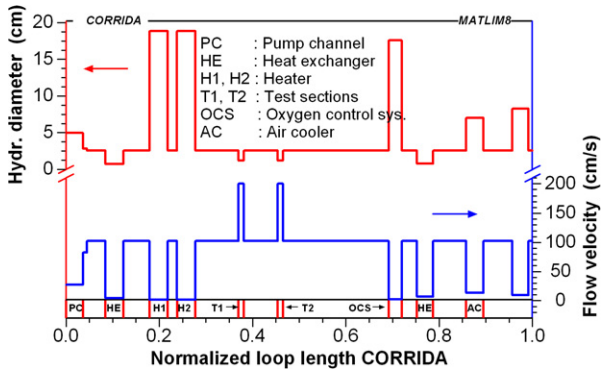

Fig. 3. Axial profiles of the hydraulic diameter and of the flow velocity for the CORRIDA loop.

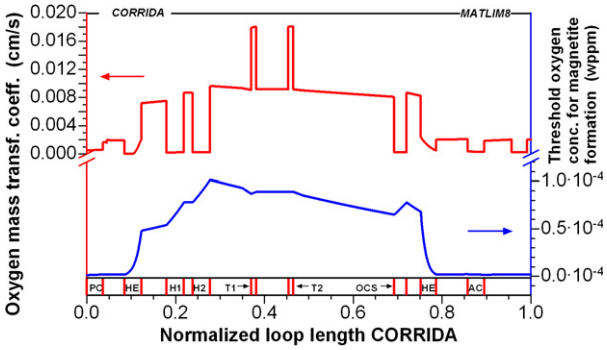

Fig. 4. Oxygen mass transfer coefficient and minimum oxygen concentration at the wall in the CORRIDA loop.

Up to now the CORRIDA loop was operated at 380 °C in the cold part and at 550 °C in the test section area, respectively. The whole temperature distribution along the loop is to be found in Fig. 5. In this figure one can also find axial profiles for the iron concentration at the channel walls for the three values of oxygen concentration. As a consequence of the solubility product over magnetite we find that the lower the oxygen concentration the higher the iron content dissolved in the liquid metal will be. For the calculation of the respective iron mass flux we have

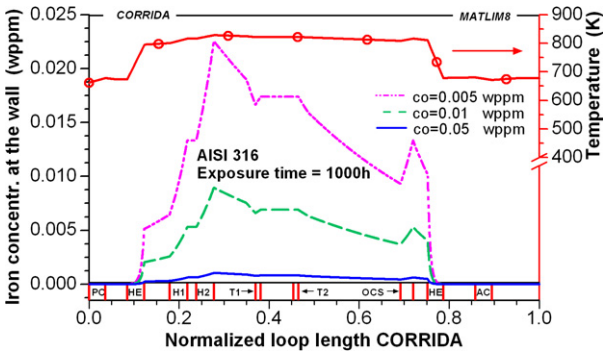

Fig. 5. Axial profiles of temperature and iron concentration at the channel walls dissolved in the liquid metal for three values of the oxygen control system.

assumed an iron diffusion coefficient in LBE of 1×10^{-6} cm^2/s (see also Refs. [12–14]).

Information on the oxygen concentration profiles along the loop (bulk and surface) as well as on dissolution/precipitation rates can be found in Figs. 6 and 7. For an input value for the oxygen level of 0.05 wppm the dissolution rates are rather low and can be neglected, but they increase with decreasing oxygen concentration. Dissolution/precipitation rates depend among others on the iron diffusion coefficient and on the solubility product over magnetite. For the time being we have no experimental data on dissolution rates of magnetite, only some hints from post test examinations that there might be an effect [25]. In case of single layer Fe/Cr scales the dissolution rates would be much lower than for magnetite decreasing with increasing Cr content. This is a consequence of the free enthalpy of formation of Fe/Cr spinel.

The mean oxygen concentration in the bulk of the liquid does not vary very much along the loop. For an input value of 0.05 wppm the variation is nearly imperceptible in the scale generated by the plot routine. It should be noted that the situation shown in Figs. 6 and 7 is for a duration of 1000 h, where oxidation is no longer progressing very fast. For the two lower input values (0.01 and 0.005 wppm) the oxygen concentration at the surface is in the high temperature leg of the loop higher than that in the bulk of the liquid metal. This is due to oxygen release by dissolution of magnetite. The low values of oxygen concentration at the surface of the structures in the cold leg of the loop are a consequence of magnetite precipitation in this axial zone.

In Fig. 8 the axial profiles of the oxide scale thickness for the three cases are plotted. The oxide scales in the cold leg

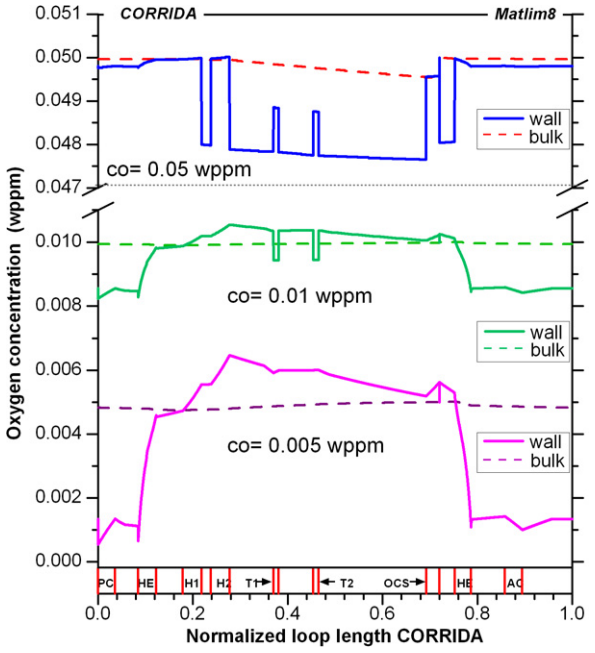

Fig. 6. Axial distributions of oxygen concentrations in the bulk of the fluid (c_O^b) and at the channel wall (c_O^w) for three values of oxygen control.

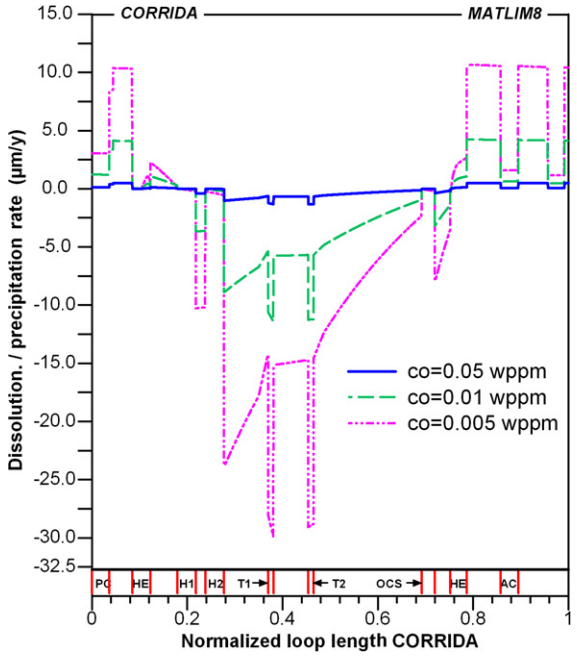

Fig. 7. Axial distributions of dissolution/precipitation rates for three values of oxygen control.

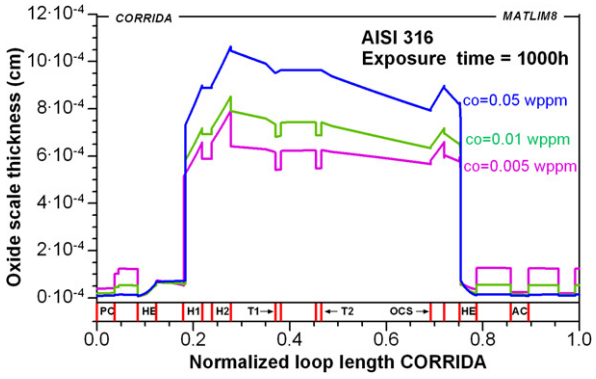

Fig. 8. Axial distributions of the oxide scale thickness for AISI 316L structural material after 1000 h operation in the CORRIDA loop for the three input values of oxygen content.

of the loop as calculated by MATLIM are entirely due to precipitation. Thus, the lower the oxygen input value by the oxygen control system the higher is the mass transfer from the hot leg to the cold leg.

9. Conclusions

Oxygen control in liquid lead and lead–bismuth loops is of great importance as the formation of protective oxide scales must under all circumstances be assured. Otherwise, severe dissolution attack of structural components is to be expected. There are certain thermo-hydraulic limitations of oxygen supply towards the structural materials. This point has not been fully treated in literature in the past. The mode of oxidation of stainless steels (single layer Fe/Cr spinel or duplex scales) does not only depend on the level of the oxygen supply system but may also be influenced by thermo-hydraulic parameters and also by the characteristics of the loop. Our analysis suggests that for moderately high values of oxygen concentration the first stage of oxidation is with slowly growing dense single layer scales. The length of this first stage should then depend on the level of oxygen content in the loop.

Evolution of oxide scales in liquid metals under forced convection flow is due to the combined effect of oxidation and of dissolution/precipitation mechanisms by the liquid metal. A main assumption of this work is that correlations for oxidation rate constants gained from tests under gas atmosphere may also be applied in liquid metals if they are in a suitable form with temperature and oxygen partial pressure at the wall as parameters. Dissolution should increase with lower oxygen content in the liquid metal and it is presumably considerably higher for magnetite than for Fe/Cr spinel scales. Evolution of oxide scales on structural materials can be calculated with the recently developed computer code MATLIM, which performs a 1-D simulation of heavy liquid metal loops like CORRIDA.

A future comparison with experimental data has to confirm whether MATLIM is able to predict the "real" materials behavior by using e.g. gas phase data for the derivation of the oxygen mass transfer coefficient in LBE.

References

[1] F. Carminati, R. Klapisch, J.P. Revol, Ch. Roche, J.A. Rubio, C. Rubbia, CERN/AT/93-47 (ET), 1993.
[2] C. Rubbia, J. Rubio, S. Buono, F. Carminati, N. Fietier, J. Galvez, C. Geles, Y. Kadi, R. Klapisch, P. Mandrillon, J.P. Revol, Ch. Roche, CERN/AT/95-44 (ET), 1995.
[3] G. Casini, J. Sannir, J. Nucl. Mater. 179–181 (1991) 47.
[4] J. Konys, W. Krauss, Z. Voss, O. Wedemeyer, J. Nucl. Mater. 1379 (2004) 329.
[5] R.C. Asher, D. Davies, S.A. Beetham, Corr. Sci. 17 (1977) 545.
[6] G. Müller, FZKA report 6422, 2000.
[7] B.F. Gromov, Yu.L. Orlov, P.N. Martynov, K.D. Ivanov, V.A. Gulevski, Physical–chemical principles of lead–bismuth coolant technology, in: H.U. Borgstedt, G. Frees (Eds.), Liquid Metal Systems, Plenum, 1995, p. 339.
[8] V. Markov, Corrosion of structural materials in PbBi and Pb, Seminar on the concept of lead-cooled fast reactor, Cadarache, 1997.
[9] G. Müller, G. Schumacher, F. Zimermann, J. Nucl. Mater. 278 (2000) 85.
[10] J. Konys, H. Muscher, Z. Voss, O. Wedemeyer, J. Nucl. Mater. 296 (2001) 289.
[11] H. Muscher, J. Konys, Z. Voss, O. Wedemeyer, FZKA report 6690, 2001.
[12] T. Malkow, H. Steiner, H. Muscher, J. Konys, J. Nucl. Mater. 335 (2004) 199.
[13] H. Steiner, J. Konys, J. Nucl. Mater. 338 (2006) 18.
[14] H. Steiner, J. Konys, FZKA report 7212, 2006.
[15] X. He, N. Li, M. Mineev, J. Nucl. Mater. 297 (2001) 214.
[16] F. Balbaud-Celerier, F. Barbier, J. Nucl. Mater. 289 (2001) 227.
[17] R. Ganesan, T. Gnanasekaran, Raman S. Srinivasa, J. Nucl. Mater. 349 (2005) 133.

[18] C.S. Tedmon Jr., J. Electrochem. Soc. 113 (1966) 766.
[19] J. Zhang, N. Li, Y. Chen, J. Nucl. Mater. 342 (2005) 1.
[20] N. Li, J. Nucl. Mater. 300 (2002) 73.
[21] I. Barin, Thermochemical Data of Pure Substances, VCH, Weinheim, 1989.
[22] M. Saito, H. Furuya, M. Sugisaki, J. Nucl. Mater. 135 (1985) 11.
[23] L. Martinelli, private communication.
[24] E.N. Fuller, P.D. Schettler, J.C. Giddings, Ind. Eng. Chem. 58 (1966) 19.
[25] C. Schroer, Z. Voß, O. Wedemeyer, J. Novotny, J. Konys, J. Nucl. Mater. 356 (2006) 189.